Kinetics of C_2 Reactions during High-Temperature Pyrolysis of Acetylene

T. Kruse and P. Roth*

Institut für Verbrennung und Gasdynamik, Gerhard-Mercator-Universität Duisburg, 47048 Duisburg, Germany

Received: October 29, 1996; In Final Form: January 3, 1997[⊗]

The kinetics of C_2 radical reactions during the first stage of acetylene high-temperature pyrolysis was studied by monitoring C, C_2 and C_3 radicals. Quantitative C_2 detection was performed by ring dye laser absorption spectroscopy, C atoms were measured by applying atomic resonance absorption spectroscopy, and C_3 radicals were monitored by their emission using a combination of a spectrograph and an intensified CCD camera system. The experiments were performed behind reflected shock waves and cover the temperature range of 2580−4650 K at pressures around 2 bar. In the first part of the study initial mixtures containing Ar with 5−50 ppm C_2H_2 were used. In this very low concentration range, rate coefficients for the following four reactions were determined: $C_2H_2 + M \overset{k_1}{\leftrightarrow} C_2H + H + M$ (R1); $C_2H + M \overset{k_2}{\rightleftharpoons} C_2 + H + M$ (R2); $C_2 + C_2 \overset{k_3}{\rightleftharpoons} C + C_3$ (R3); $C_2 + M \overset{k_4}{\rightleftharpoons} C + C + M$ (R4); where $k_1 = 6.96 \times 10^{39}\ T^{-6.06} \exp(-67\,130/T)$ cm^3 mol^{-1} s^{-1}, $k_2 = 1.74 \times 10^{35}\ T^{-5.16} \exp(-57\,367/T)$ cm^3 mol^{-1} s^{-1}, $k_3 = 3.2 \times 10^{14}$ cm^3 mol^{-1} s^{-1}, and $k_4 = 1.5 \times 10^{16} \exp(-71\,650/T)$ cm^3 mol^{-1} s^{-1}. Furthermore, this experiments indicate that a modification of the JANAF[1] thermodynamic data of either C, C_2 or C_3 seems to be necessary. In the second part, some experiments with relatively high initial acetylene concentrations up to 500 ppm C_2H_2 in Ar were carried out to check the validity of a more complex mechanism for the acetylene pyrolysis. Finally in a third part, a perturbation study was performed by adding 1000 ppm H_2 to the initial mixtures of Ar with 20 and 50 ppm of C_2H_2. For the most important perturbation reactions, $C_2 + H_2 \overset{k_5}{\rightleftharpoons} C_2H + H$ (R5) and $C_2H + H_2 \overset{k_6}{\rightleftharpoons} C_2H_2 + H$ (R6), rate coefficients of $k_5 = 6.6 \times 10^{13} \exp(-4000/T)$ cm^3 mol^{-1} s^{-1} and $k_6 = 7.4 \times 10^{14} \exp(-3400/T)$ cm^3 mol^{-1} s^{-1} were obtained.

Introduction

Elementary reactions involving C_2 radicals and other small carbon species like C and C_3 play an important role in the high-temperature chemistry of hydrocarbons. Examples are soot formation in hot flames, diamond synthesis from gas phase pyrolysis, or the formation and decay of the recently discovered C_{60} fullerene.[2−4] The pyrolysis of acetylene has been studied in the last decades by numerous investigators, but up to now, no quantitative measurement of C, C_2, or C_3 radicals has been performed. Only in one kinetic study by Beck et al.,[5] C_2 radicals were measured during the acetylene pyrolysis, but in this investigation C_2 was monitored only by emission and thus only qualitatively. With the development of tunable and narrow bandwith CW ring dye lasers, the sensitive and quantitative detection of many di- and some triatomic molecules by direct absorption measurements became feasible.

In the present study, C_2 radicals were detected by ring dye laser absorption spectroscopy (RDLAS) using selected rotational transitions in the (1−0) and (0−0) bands of the C_2 ($d^3\Pi_g \leftarrow a^3\Pi_u$) Swan system. To reveal the reaction mechanism, some additional experiments were made by recording C and C_3 concentrations by atomic resonance absorption spectroscopy (ARAS) and emission spectroscopy, respectively. The combination of this spectroscopic methods with the shock tube technique allowed direct observation of several C_2 reactions.

Experimental Section

The experiments were performed behind reflected shock waves in a stainless steel shock tube of 80 mm inner diameter; see Figure 1. The tube is constructed as heatable ultrahigh-vacuum apparatus and can be evacuated down to pressures below 5×10^{-8} mbar by a turbo-molecular pump. The shock wave is formed after bursting of aluminum diaphragms, which were 50 or 70 μm thick. Temperatures and pressures behind the reflected shock waves were calculated, on the basis of one-dimensional gas dynamic equations, from the speed of the incident shock wave, which was measured by four piezoelectric pressure gauges. The gases used were carefully mixed in a stainless steel cylinder by the partial pressure method. They were of the highest commercially available purity; i.e., Ar (99.9999%), H_2 (99.9999%), and C_2H_2 (99.6%). In a few experiments the acetylene was passed through an activated carbon filter to remove the traces of 0.4% acetone, but this experiments showed no difference from the ones with unpurified acetylene. This is in agreement with earlier studies (see, e.g., refs 6 or 7 that also showed no significant influence of acetone impurities on the kinetics of acetylene pyrolysis at low relative concentrations.

The laser spectrometer (see Figure 1), used to measure the C_2 concentration, consists of a CW ring dye laser from Spectra Physics, Model 380D, pumped by an Ar^+ laser. To realize single-mode operation, the frequency was controlled and stabilized by a reference interferometer located in a feedback loop. For a further improvement of the detection limit, an external intensity stabilization was employed. The dye laser operates under these conditions with a line width below 500 kHz and an intensity fluctuation below 1%. The laser beam was coupled into the measurement plane of the stock tube via an optical fiber and was split into probe and reference beam prior to the shock tube. Two Si photodetectors were used in the differential technique to monitor the C_2 absorption. The time absorption of about 3 μs is limited by the beam diameter and the shock speed.

[⊗] Abstract published in *Advance ACS Abstracts,* February 15, 1997.

S1089-5639(96)03373-7 CCC: $14.00

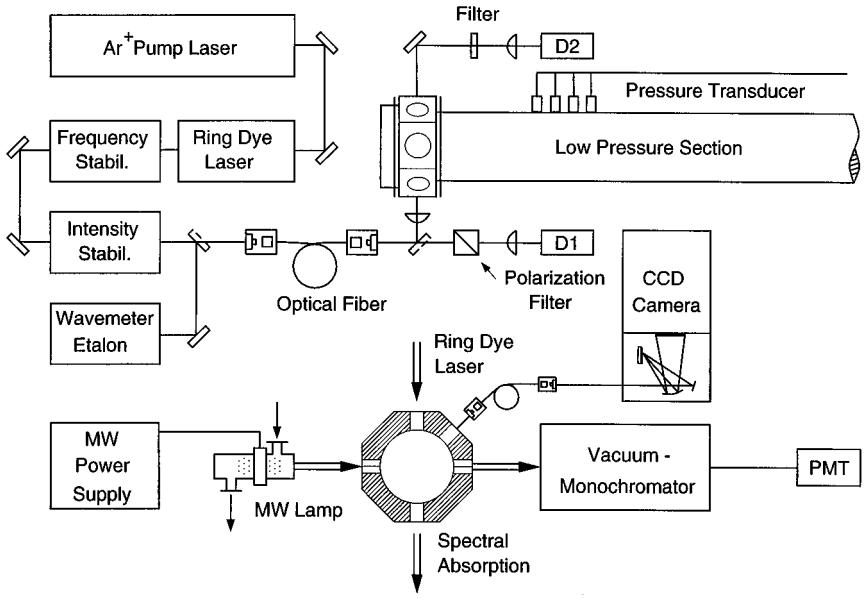

Figure 1. Experimental setup.

The C_2 concentrations were measured at two different wavelengths in the $d^3\Pi_g \leftarrow a^3\Pi_u$ Swan system:

(1) at $\lambda = 467.440$ nm corresponding to the center of the three overlapping rotational lines $R_1(37)$, $R_2(36)$, and $R_3(35)$ in the (1−0) band,

(2) at $\lambda = 516.646$ nm corresponding to the band head of the (0−0) band, consisting of nine overlapping rotational lines. The line positions were taken from ref 8, and the pressure broadening was checked by scanning each line in frequency steps of 0.02 cm^{-1} in a series of shock-tube experiments and was found to be in agreement with ref 9. Additional measurements of C_2 performed at four other lines in the (1−0) and (0−0) bands were in good agreement with the earlier described experiments.

The oscillator strengths of the C_2 Swan system, measured in the previous decades in numerous experiments, show some discrepencies. Most recent results by refs 10−12 obtained from lifetime measurements recommend a value around $f_{00} = 0.032$, which is significantly higher than the older value of $f_{00} = 0.025$ deduced from C_2 emission behind shock waves (see, e..g., refs 13 or 14. To overcome this difficulty, we have performed oscillator-strength measurements of the C_2 Swan system in some shock tube experiments; see also ref 15. The very low detection limit of less than 0.1 ppm C_2, which could be achieved with the RDLAS at $\lambda = 516.646$ nm in the (0−0) band head, allows us a direct calibration of the C_2 absorption cross section and therewith determination of the oscillator strength. At very low C_2H_2 concentrations of 2 ppm or less and temperatures above 3500 K it can be assumed, even without a detailed knowledge of the kinetics, that the C_2 formation due to two successive H atom abstractions is much faster than any subsequent C_2 consumption reactions. Thus, the maximum C_2 concentration must be equal to the initial C_2H_2 concentration. In a series of 15 shock tube experiments with initial C_2H_2 concentrations between 0.5 and 2 ppm an oscillator strength of $f_{00} = 0.037 \pm 0.002$ was determined, which is about 15% higher than the value obtained from the lifetime measurements. For the evaluation of the later described kinetic experiments we used our own f_{00} value, although the kinetic results are not significantly different when using the recent-literature value. With the knowledge of the oscillator strength together with the pressure-broadening factor, the absolute C_2 concentration could directly be determined from the measured absorption by applying the Lambert−Beer law.

C atoms were detected at $\lambda = 156.1$ nm by atomic resonance absorption spectroscopy (ARAS). A microwave discharge lamp, which was operated at 6 mbar in a mixture of He containing 1% CO, was used as the source for CI spectral radiation. A McPherson 0.5 m vacuum monochromator with a 100 μm slit combined with a photoelectron multiplier was used to select the respective C atom line. Since the spectral shapes of the lines emitted by the discharge lamp are not known precisely, the relation between the measured absorption and corresponding C atom concentration was obtained by calibration experiments based on thermal decomposition of CH_4 at temperatures $T \geq 3800$ K. For example, an absorption of 50% corresponds to a C atom concentration of about 8×10^{12} cm^{-3}.

The time-resolved emission during C_2H_2 thermal decomposition in the wavelength range from 330 to 600 nm was recorded with a combination of a grid spectrograph and an intensified CCD camera. The spectral resolution was about 2 nm and the time resolution was 20 μs during a measurement time of 1 ms. A detailed description of this system is given in ref 16.

Results

The experiments on acetylene pyrolysis were performed with mixtures of argon containing 5−500 ppm C_2H_2 at temperatures 2580 K $\leq T \leq$ 4650 K and pressures between 1.5 and 2.7 bar. In an additional series of experiments 1000 ppm H_2 was added to initial mixture containing 20 or 50 ppm C_2H_2. The present results can be grouped in three parts:

(a) experiments in mixtures containing 5−50 ppm C_2H_2, where C_2 concentrations (RDLAS), C concentrations (ARAS), and C_3 concentrations (CCD) were measured,

(b) experiments in mixtures containing 100−500 ppm C_2H_2, where only C_2 was measured, and

(c) perturbation experiments in mixtures of argon with 20 or 50 ppm C_2H_2, where the formation of C_2 was perturbed by the addition of 1000 ppm H_2 to the initial mixture.

Typical C_2 concentration profiles belonging to the first group of experiments are shown in Figure 2 for three different temperatures and an initial C_2H_2 concentration of 50 ppm diluted in Ar. The directly measured ring dye laser absorption profiles were converted via the Lambert−Beer law into concentrations based on $f_{00} = 0.037$. The noisy drawn lines belong to the experiments, and the dotted lines represent computer simulations, which will be discussed later. After a fast rise, all profiles

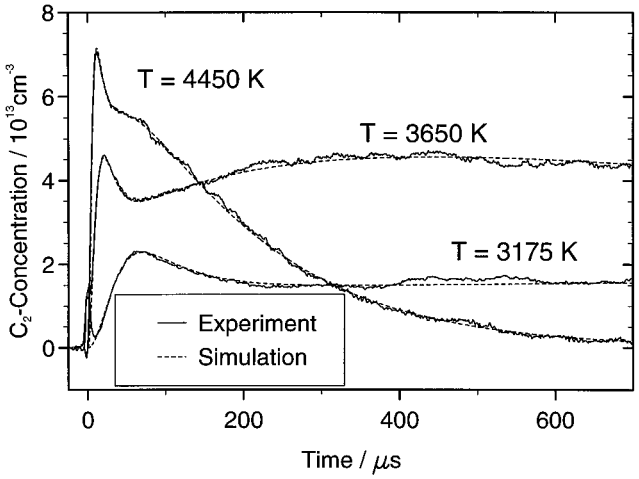

Figure 2. Measured and calculated C_2 concentration profiles at three different temperatures obtained during pyrolysis of 50 ppm C_2H_2 diluted in Ar.

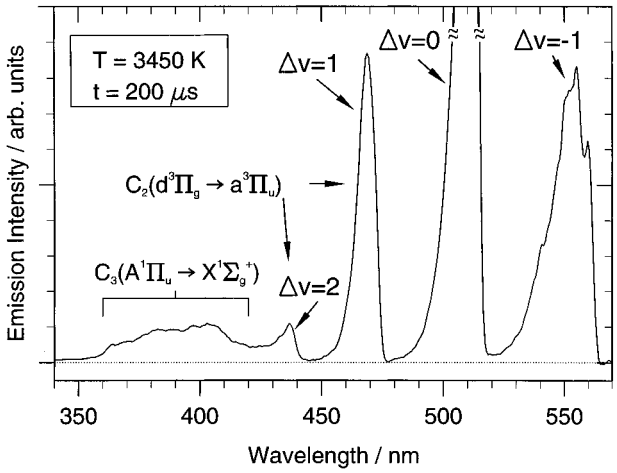

Figure 3. Emission spectrum of C_2 and C_3 during acetylene pyrolysis at a reaction time of 200 μs. Initial mixture: 10 ppm C_2H_2 diluted in Ar.

drop rapidly to about 85% of the peak concentration. In the two experiments with temperatures below 4000 K, and C_2 concentration reaches a nearly constant level after the initial peak, whereas the signal of the $T = 4450$ K experiment shows a further decrease within the observation time.

To clarify the origin of the initial peak in the C_2 absorption, additional experiments with ARAS and the CCD camera were performed. Figure 3 shows an emission spectrum obtained during the thermal decomposition of 10 ppm acetylene in argon at $T = 3450$ K. It was recorded at a reaction time of 200 μs. Two main features are of importance: the strong emission of the $C_2(d^3\Pi_g \leftarrow a^3\Pi_u)$ Swan bands at $\lambda > 430$ nm and the weak emission of the $C_3(A^1\Pi_u \leftarrow X^1\Sigma_g^+)$ bands in the spectral range 360 nm $< \lambda <$ 420 nm.[17] These emission spectra can be evaluated in order to get quantitative C_3 concentration profiles. For this purpose, the emission signals $\epsilon(\lambda)$ of the $\Delta v = 0$ progressions of C_2 and the $A^1\Pi_u \leftarrow X^1\Sigma_g^+$ transition of C_3 were integrated with respect to the wavelength at a fixed time τ for each experiment. The integrated emission intensities $I_{C_2}^{(\tau)}$ and $I_{C_3}^{(\tau)}$ at a fixed time τ were defined as

$$I_{C_2}^{(\tau)} = \int_{480\text{ nm}}^{522\text{ nm}} \epsilon^{(\tau)}(\lambda)\, d\lambda \qquad I_{C_3}^{(\tau)} = \int_{350\text{ nm}}^{420\text{ nm}} \epsilon^{(\tau)}(\lambda)\, d\lambda$$

with $\epsilon^{(\tau)}(\lambda)$ being the wavelength dependent emission at $t = \tau$. With the knowledge of the simultaneously measured C_2 concentration by the RDLAS, the C_3 concentration can be calibrated at the time τ by

$$\frac{I_{C_3}^{(\tau)}}{I_{C_2}^{(\tau)}} = \frac{[C_3]^{(\tau)}}{[C_2]^{(\tau)}} \frac{f_{el,C_3}\, \nu_{C_3}^3 \exp(-hc\nu_{C_3}/kT)}{\sum_i f_{ii,C_2}\, \nu_{ii,C_2}^3 \exp(-hc\nu_{ii,C_2}/kT)}$$

whereby the sum must be taken over the progression of the C_2 bands, and ν_{C_3} and ν_{ii,C_2} are the respective mean band wavenumbers of C_3 and C_2. The electronic oscillator strength f_{el,C_3} was taken from ref 18 and f_{ii,C_2} was calculated from the measured f_{00} oscillator strength of C_2 using the Franck−Condon factors q_{ii,C_2} given in ref 19. After calibration of the C_3 emission against C_3 concentration at one fixed time τ, the proportionality factor between emission and concentration of C_3 is known for the whole time scale of this specific shock tube experiment. A typical result of a C_3 concentration profile obtained from an emission signal is shown in Figure 4 together with a C_2 profile and a C atom concentration profile (see open circles) obtained by ARAS. The experimental conditions are 10 ppm C_2H_2, $T = 3450$ K, and $p = 2.2$ bar. The decrease in the C_2 concentration at early reaction time is accompanied by an increase in C_3 and C atom concentration. At later reaction times, the concentration of all three species reach a nearly constant level. The computer simulation shown in Figure 4 as dotted lines will be discussed later.

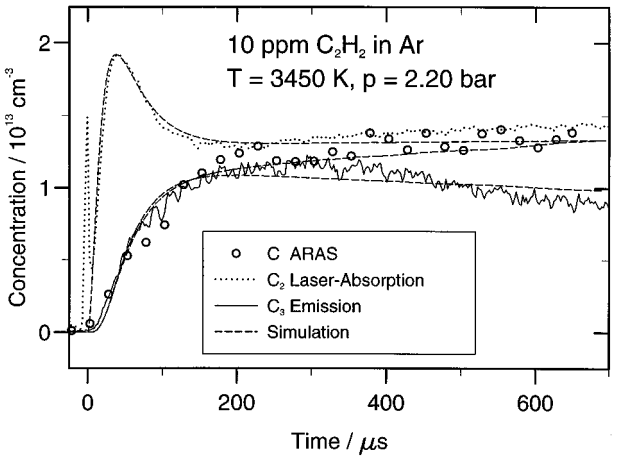

Figure 4. Measured and calculated C, C_2, and C_3 concentrations during pyrolysis of 10 ppm acetylene diluted in Ar.

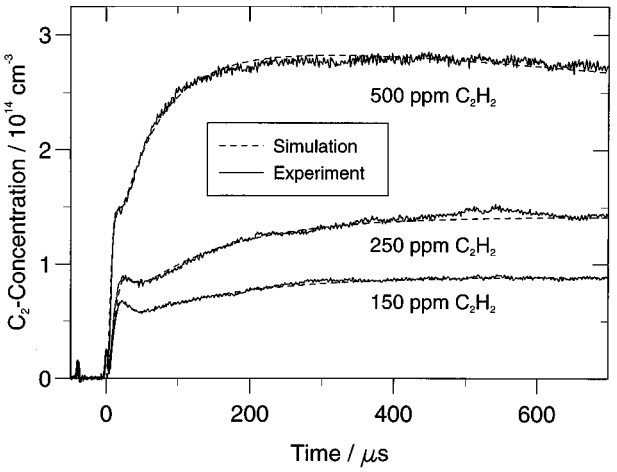

Figure 5. C_2 concentration profiles obtained from experiments with different initial C_2H_2 concentrations at temperatures around 3500 K and pressures of about 2 bar, in comparison with computer simulation.

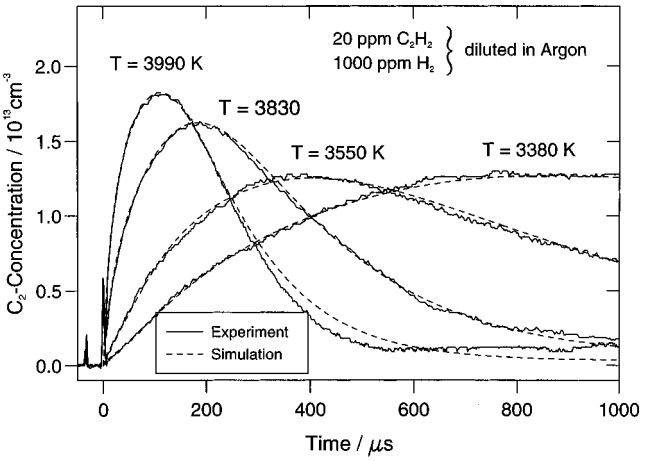

Figure 6. Measured and calculated C_2 concentration profiles at four different temperatures obtained from the pyrolysis of 20 ppm C_2H_2 diluted in Ar perturbated by the addition of 1000 ppm H_2.

The second group of pyrolysis experiments was performed in mixtures containing 100−500 ppm C_2H_2 diluted in Ar. The reason for chosing this higher initial concentrations was to verify existing kinetic models for C_2H_2 pyrolysis by comparing calculated C_2 profiles with measured ones. Three typical measured C_2 profiles from a total of about 10 experiments are shown in Figure 6; see noisy lines. At time $t \approx 0$ C_2 increases very rapidly, but different from the low C_2H_2 concentration experiments, the initial C_2 peak structure diminishes with increasing initial C_2H_2 concentration nearly completely. Furthermore, a second slower C_2 increase appears, which reaches a flat maximum or a constant level after some 100 μs. The result of all experiments together with the experimental conditions are summarized in Table 1.

The last group of experiments includes perturbation of C_2H_2 pyrolysis by H_2. Four examples of measured C_2 profiles in mixtures of Ar with 20 ppm C_2H_2 and 1000 ppm H_2 are shown in Figure 6. The peaks at $t = 0$ and $t < 0$ are schlieren signals caused by the incident and reflected shock wave when passing through the laser beam. The structure of the C_2 signals is very different from those of the H_2-free mixtures. A direct comparison of measured C_2 profiles obtained at identical temperatures of $T = 3380$ K from a mixture of 20 ppm C_2H_2 diluted in argon with Figure 6) and without (Figure 7) addition of H_2 clearly illustrates this effect. As a result of the H_2 addition, the initial rapid increase in the C_2 formation (see Figure 7) is very moderate in Figure 6 and the initial peak at $t \approx 40$ μs disappears completely. Also the maximum amount of C_2 formed is different in Figures 6 and 7 by a factor of 1.8. In general the H_2 addition attenuates the C_2 formation during pyrolysis of C_2H_2. The results of all experiments together with the experimental conditions are also summarized in Table 1.

Discussion

It seems useful to discuss the experimental observations during pyrolysis of C_2H_2 within the meaning of the three groups of experiments introduced earlier.

The very rapid formation of C_2 during high-temperature pyrolysis of acetylene at low relative C_2H_2 concentrations (group I experiments), as shown in Figures 2 and 4, can kinetically be understood by a successive abstraction of H atoms:

$$C_2H_2 + M \overset{1}{\rightleftharpoons} C_2H + H + M \qquad \text{(R1)}$$

$$C_2H + M \overset{2}{\rightleftharpoons} C_2 + H + M \qquad \text{(R2)}$$

The results of Figure 4 also clearly indicate a strong formation of both C and C_3 during the time of about 100 μs, when the initial C_2 peak decreases to a nearly constant concentration level. It seems quite obvious to interpret this behavior by the bimolecular reaction:

$$C_2 + C_2 \overset{3}{\rightleftharpoons} C + C_3 \qquad \text{(R3)}$$

Furthermore, the observed additional decrease in the C_2 concentration at temperatures $T > 4000$ K during the whole observation time of 700 μs (see Figure 2) suggests a dissociation of C_2:

$$C_2 + M \overset{4}{\rightleftharpoons} C + C + M \qquad \text{(R4)}$$

For the computer simulation of the measured C_2 time histories, this simple mechanism was extended by additional reactions listed in Table 2, which have, however, only a very minor influence for initial C_2H_2 concentrations of 50 ppm or less.

A problem is that the experimentally observed steady state C_2 concentration at later reaction times (see Figures 2 and 4) is significantly higher than the calculated value. An example is given in Figure 7. The dotted line represents the calculated C_2 concentration, which is for times $t > 100$ μs significantly below the measured steady state value. This is due to the JANAF thermodynamic data[1] for C, C_2, and C_3, which are equal to those given in ref 20. For the example given in Figure 7 these literature data yield an equilibrium constant of $K_{c,3} = 10$. The best fit to the experiments however can be obtained with an equilibrium constant of $K_{c,3} = 1.9$, which increases the importance of the backward reaction R3; see Figure 7. This can be achieved by either increasing the Gibbs free energies of C or C_3 by 11 kcal or by decreasing the value of C_2 by 5.5 kcal or by a combination of both. A change in the Gibbs free energy can be obtained either by a change in the enthalpies or the entropies of the species. Since the necessary variation in $\Delta G°$ is constant over the studied temperature range between 2580 and 4650 K, it seems near at hand to attribute it to changes in the enthalpies rather than in the entropies of the species. Recently Urdahl et al.[21] determined experimentally a value for the heat of formation of C_2, which is by about 4 kcal/mol lower than the JANAF value. A lower value was also recommended in a theoretical study.[22] Therefore and for reasons discussed later, we think that a reduction of the JANAF value[1] for the enthalpy of C_2 by about (5.5 ± 0.5) kcal mol^{-1} corresponding to a change in the heat of formation from $\Delta_f H^0_{298.15} = 200.2$ kcal mol^{-1} to $\Delta_f H^0_{298.15} = 194.7$ kcal mol^{-1} is most likely to fullfill the requirements of the equilibrium constant of reaction R3.

With the above mechanism and the modification in the thermodynamic data of C_2, it is possible to fit the measured C_2 profiles. It is clear that the rapid initial C_2 increase is mainly sensitive to reactions R1 and R2. A value for the rate coefficient k_1 is given by ref 23 for the temperature range 1850 K ≤ T ≤ 3500 K on the basis of experiments of Frank and Just.[6] In a first attempt we used this rate coefficient and modified only k_2 to fit the initial C_2 increase. As indicated in Figure 8 the initial C_2 increase could not be fitted satisfactorly, especially for temperatures below 3200 K. Moreover, the resulting rate coefficient k_2 necessary to fit the further parts of the C_2 profiles showed an extraordinary small activation energy around 67 kcal, which is only 57% of the reaction enthalpy for R2. We therefore started to fit the measured C_2 profiles by varying both rate coefficients k_1 and k_2 of the above mechanism. This results in nearly perfect fits of the experimental traces, even for the colder experiments; see Figure 8. The resulting rate coefficients k_1

TABLE 1: Experimental Conditions and Characteristics of Measured C_2 Concentration Profiles Obtained during High-Temperature Pyrolysis of Acetylene Highly Diluted in Ar

T (K)	p (bar)	$[C_2H_2]_0$ (ppm)	t_{peak} (μs)	$[C_2]_{peak}$ (cm^{-3})	$[C_2]_{100\mu s}$ (cm^{-3})	$[C_2]_{300\mu s}$ (cm^{-3})	$[C_2]_{600\mu s}$ (cm^{-3})
3082	2.24	5.	155	6.2×10^{12}	5.4×10^{12}	4.8×10^{12}	3.0×10^{12}
3225	2.15	5	105	8.2×10^{12}	8.2×10^{12}	4.7×10^{12}	4.0×10^{12}
3431	2.05	5	61	1.0×10^{13}	8.5×10^{12}	4.5×10^{12}	4.2×10^{12}
3501	2.27	5	49	1.1×10^{13}	7.8×10^{12}	5.2×10^{12}	5.0×10^{12}
3552	2.16	5	43	1.2×10^{13}	8.0×10^{12}	5.7×10^{12}	5.5×10^{12}
3610	2.09	5	40	1.3×10^{13}	9.5×10^{12}	6.0×10^{12}	5.9×10^{12}
2580	2.45	10	540	2.3×10^{12}	1.5×10^{11}	1.3×10^{11}	2.2×10^{12}
2580	2.45	10	520	2.5×10^{12}	2.0×10^{11}	1.4×10^{12}	2.4×10^{12}
2580	2.45	10	520	2.5×10^{12}	2.0×10^{11}	1.4×10^{12}	2.4×10^{12}
2626	2.51	10	490	2.8×10^{12}	2.0×10^{11}	1.8×10^{12}	2.5×10^{12}
2685	2.27	10	450	2.9×10^{12}	4.5×10^{11}	2.3×10^{12}	2.5×10^{12}
2775	2.49	10	305	5.2×10^{12}	2.2×10^{12}	5.1×10^{12}	4.1×10^{12}
2824	2.41	10	235	5.8×10^{12}	3.0×10^{12}	5.4×10^{12}	3.9×10^{12}
2850	2.12	10	225	5.4×10^{12}	2.8×10^{12}	5.0×10^{12}	3.8×10^{12}
2866	2.35	10	250	4.9×10^{12}	2.5×10^{12}	4.8×10^{12}	3.7×10^{12}
3018	2.12	10	150	6.8×10^{12}	6.2×10^{12}	5.5×10^{12}	4.0×10^{12}
3053	2.31	10	100	1.1×10^{13}	1.1×10^{13}	6.2×10^{12}	5.2×10^{12}
3062	2.40	10	130	8.5×10^{12}	7.9×10^{12}	6.1×10^{12}	4.9×10^{12}
3113	2.40	10	113	9.6×10^{12}	9.5×10^{12}	6.4×10^{12}	5.6×10^{12}
3150	2.06	10	105	9.0×10^{12}	9.0×10^{12}	6.0×10^{12}	5.1×10^{12}
3281	1.95	10	80	1.1×10^{13}	1.1×10^{13}	6.5×10^{12}	6.1×10^{12}
3293	1.99	10	73	1.3×10^{13}	1.1×10^{13}	6.7×10^{12}	6.3×10^{12}
3345	2.40	10	55	1.6×10^{13}	1.3×10^{13}	8.4×10^{12}	8.4×10^{12}
3365	2.17	10	57	1.5×10^{13}	1.2×10^{13}	8.3×10^{12}	8.4×10^{12}
3450	2.20	10	40	1.9×10^{13}	1.4×10^{13}	1.4×10^{13}	1.4×10^{13}
3523	2.02	10	40	1.8×10^{13}	1.2×10^{13}	8.2×10^{12}	9.0×10^{12}
3652	2.09	10	31	2.1×10^{13}	1.3×10^{13}	1.2×10^{12}	1.2×10^{12}
3773	2.02	10	26	2.2×10^{13}	1.3×10^{13}	1.2×10^{13}	1.2×10^{13}
3830	1.98	10	23	2.2×10^{13}	1.2×10^{13}	1.3×10^{13}	1.2×10^{13}
4061	0.76	10	30	9.2×10^{12}	6.8×10^{12}	5.0×10^{12}	4.8×10^{12}
4155	1.92	10	14	2.4×10^{13}	1.3×10^{13}	1.2×10^{13}	8.5×10^{12}
4380	1.80	10	10	2.5×10^{13}	1.1×10^{13}	5.0×10^{12}	1.2×10^{12}
4575	0.75	10	18	9.3×10^{12}	5.1×10^{12}	2.7×10^{12}	8.0×10^{11}
3382	2.18	20	45	2.1×10^{13}	1.6×10^{13}	1.3×10^{13}	1.3×10^{13}
3558	2.15	20	30	2.8×10^{13}	1.8×10^{13}	1.7×10^{13}	1.7×10^{13}
3734	1.98	20	23	3.2×10^{13}	1.9×10^{13}	2.1×10^{13}	2.2×10^{13}
2945	2.14	50	121	1.7×10^{13}	1.6×10^{13}	1.1×10^{13}	1.0×10^{13}
2999	2.23	50	118	1.7×10^{13}	1.5×10^{13}	1.2×10^{13}	1.2×10^{13}
3175	2.23	50	63	2.4×10^{13}	2.1×10^{13}	1.6×10^{13}	1.6×10^{13}
3483	2.11	50	32	3.8×10^{13}	2.9×10^{13}	3.2×10^{13}	3.5×10^{13}
3650	1.92	50	22	4.6×10^{13}	3.7×10^{13}	4.2×10^{13}	4.2×10^{13}
3745	1.97	50	18	5.2×10^{13}	4.0×10^{13}	4.5×10^{13}	4.3×10^{13}
3808	2.01	50	16	5.8×10^{13}	4.4×10^{13}	4.7×10^{13}	4.8×10^{13}
3931	2.09	50	12	6.8×10^{13}	4.5×10^{13}	4.7×10^{13}	4.8×10^{13}
3976	2.04	50	12	6.8×10^{13}	4.5×10^{13}	4.6×10^{13}	4.2×10^{13}
3990	1.98	50	11	6.9×10^{13}	4.7×10^{13}	4.9×10^{13}	4.0×10^{13}
4085	1.98	50	16	7.3×10^{13}	5.8×10^{13}	4.9×10^{13}	3.0×10^{13}
4189	1.89	50	11	7.5×10^{13}	5.8×10^{13}	4.0×10^{13}	1.6×10^{13}
4280	1.85	50	10	7.7×10^{13}	5.5×10^{13}	3.2×10^{13}	1.0×10^{13}
4403	1.83	50	9	7.3×10^{13}	5.0×10^{13}	1.9×10^{13}	3.1×10^{12}
4437	1.83	50	9	7.4×10^{13}	4.8×10^{13}	1.6×10^{13}	2.5×10^{12}
4450	1.82	50	9	7.2×10^{13}	4.9×10^{13}	1.7×10^{13}	2.7×10^{12}
4518	1.71	50	9	7.8×10^{13}	4.0×10^{13}	8.0×10^{12}	1.0×10^{12}
4609	1.60	50	7	7.4×10^{13}	3.5×10^{13}	3.0×10^{12}	5×10^{11}
4634	1.58	50	6	7.2×10^{13}	3.0×10^{13}	2.0×10^{12}	2×10^{11}
3489	2.10	75	26	4.6×10^{13}	3.9×10^{13}	4.9×10^{13}	5.1×10^{13}
3572	2.17	100	22	6.2×10^{13}	5.0×10^{13}	6.3×10^{13}	6.3×10^{13}
3510	2.14	125	22	6.3×10^{13}	6.2×10^{13}	7.9×10^{13}	8.5×10^{13}
3509	2.12	150	22	6.3×10^{13}	6.1×10^{13}	7.3×10^{13}	8.7×10^{13}
3430	2.21	200	22	7.9×10^{13}	8.8×10^{13}	1.1×10^{14}	1.2×10^{14}
3360	2.01	250	24	9.1×10^{13}	9.5×10^{13}	1.3×10^{14}	1.5×10^{14}
3250	2.06	500	40	1.2×10^{14}	1.6×10^{14}	2.0×10^{14}	$2.2q \times 10^{14}$
3490	2.13	500	18	1.5×10^{14}	2.5×10^{14}	2.8×10^{14}	2.7×10^{14}
3605	1.90	500	13	1.6×10^{14}	2.4×10^{14}	2.5×10^{14}	2.6×10^{14}
3785	1.83	500	11	1.7×10^{14}	3.2×10^{14}	3.7×10^{14}	3.4×10^{14}

T (K)	p (bar)	$[C_2H_2]_0$ (ppm)	$[H_2]_0$ (ppm)	t_{peak} (μs)	$[C_2]_{peak}$ (cm^{-3})	$[C_2]_{100\mu s}$ (cm^{-3})	$[C_2]_{300\mu s}$ (cm^{-3})	$[C_2]_{600\mu s}$ (cm^{-3})
2890	2.13	20	1000			1.0×10^{11}	2.0×10^{11}	7.0×10^{11}
3380	2.22	20	1000			3.2×10^{12}	8.1×10^{12}	1.2×10^{13}
3550	1.85	20	1000	395	1.3×10^{13}	6.3×10^{12}	1.3×10^{13}	1.1×10^{13}
3830	1.91	20	1000	195	1.6×10^{13}	1.4×10^{13}	1.5×10^{13}	5.1×10^{12}
3990	1.82	20	1000	110	1.8×10^{13}	1.8×10^{13}	7.2×10^{12}	1.5×10^{12}
3128	2.23	50	1000			1.9×10^{12}	6.9×10^{12}	1.3×10^{13}
3378	2.19	50	1000			6.3×10^{12}	1.7×10^{13}	2.7×10^{13}
3440	1.97	50	1000			9.5×10^{12}	2.0×10^{13}	2.7×10^{13}
3440	1.97	50	1000			9.5×10^{12}	2.0×10^{13}	2.7×10^{13}
3700	1.95	50	1000	260	2.6×10^{13}	1.8×10^{13}	2.5×10^{13}	1.2×10^{13}
3810	1.83	50	1000	150	2.3×10^{13}	2.0×10^{13}	1.6×10^{13}	4.0×10^{12}

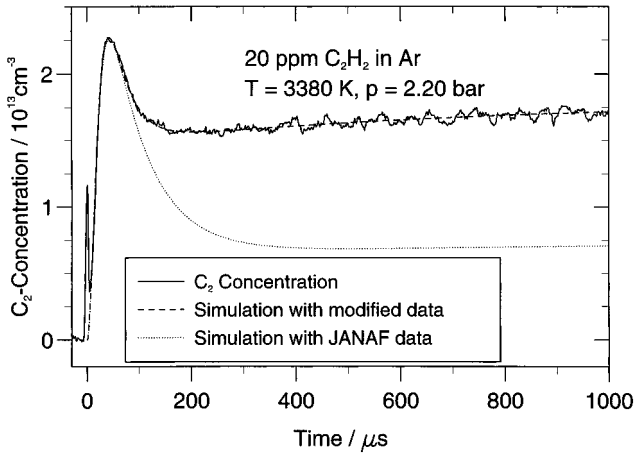

Figure 7. Simulation of C_2 concentration profiles with original and modified thermodynamic data for an experiment with 20 ppm C_2H_2 diluted in Ar.

and k_2 obtained from a total of 38 experiments are summarized in Figures 9 and 10. The points for k_1 show a weak non-Arrhenius behavior, which can in the lower temperature regime be represented by an activation energy of about 104 kcal mol^{-1}. For the whole temperature range 2580 K $\leq T \leq$ 3830 K a good fit to the experiments is possible by the modified Arrhenius expression:

$$k_1 = 6.96 \times 10^{39}\, T^{-6.06} \exp(-67\,130/T)\ \mathrm{cm^3\ mol^{-1}\ s^{-1}}$$

Our results for k_1 at 3000 K is by a factor of 2 higher than the value of Frank and Just.[6]

The data points for the rate coefficient k_2, summarized in Figure 10, can be represented by the Arrhenius expression:

$$k_2 = 1.1 \times 10^{15} \exp(-41\,868/T)\ \mathrm{cm^3\ mol^{-1}\ s^{-1}}$$

The relatively low activation energy of 83 kcal favors the suggested reduction in the heat of formation for C_2. A modified Arrhenius expression similar to that of k_1 based on the heat of reaction for reaction R2 of 114 kcal mol^{-1} would result in a temperature exponent of -5.16.

The rate coefficients of the bimolecular reaction R3 and the thermal decomposition reaction R4 were also determined by computer fittings from the measured C_2 concentration profiles. Individual results obtained are summarized in Figures 11 and 12. They can be represented by the Arrhenius expressions:

$$k_3 = (3.2 \pm 0.4) \times 10^{14}\ \mathrm{cm^3\ mol^{-1}\ s^{-1}}$$

$$k_4 = (1.5 \pm 0.5) \times 10^{16} \exp(-71\,660/T)\ \mathrm{cm^3\ mol^{-1}\ s^{-1}}$$

The rate coefficient k_3 was found to be independent of temperature. The activation energy of reaction R4 of 142 $\pm$ 5 kcal mol^{-1} is in good agreement with published values for the C_2 bond dissociation energy; see, e.g., refs 21 and 24−27, and the values resulting from the thermodynamic data of C and C_2. All computer simulations for obtaining the given rate coefficients k_1−k_4 were performed both with the reaction mechanism R1−R4 and with the more extended mechanism listed in Table 2. The results were nearly the same.

The interpretation of the group II experiments with higher initial C_2H_2 concentrations of 100−500 ppm (see examples in Figure 6) needs an extension of the thermal decomposition mechanism. We started with a system of 145 elementary reactions, mainly taken from Kiefer et al., refs 28 and 29. By careful sensitivity analysis, the 60 reactions listed in Table 2 were found to have influence on the measured C_2 profiles. Reactions R1−R4 are identical to those discussed earlier, and the rate coefficients of R5 and R6 will be discussed later. It was found that the second, slower C_2 increase observed in Figure 5 is mainly sensitive to the reactions R12, R52, R19, R36, and R14 involving the species C_2, C_2H, C_4, C_4H, C_6, and C_6H. Since many of the sensitive reactions have equilibrium constants close to 1, the thermodynamic properties, i.e., the Gibbs free energies, of this species become very important for these experimental conditions. The thermodynamic properties at 3500 K of some

TABLE 2: Simplified Reaction Mechanism for the High-Temperature Pyrolysis of Acetylene[a]

	reaction	A/cm^3 mol^{-1} s^{-1}	n	E_A/ (cal/mol)	ref
1	$C_2H_2 + M \rightleftharpoons C_2H + H + M$	6.96×10^{39}	−6.06	133 400.	s.t.
2	$C_2H + M \rightleftharpoons C_2 + H + M$	1.74×10^{35}	−5.16	114 000.	s.t.
3	$C_2 + C_2 \rightleftharpoons C_3 + C$	3.20×10^{14}	0.	0.	s.t.
4	$C_2 + M \rightleftharpoons C + C + M$	1.50×10^{16}	0.	142 400.	s.t.
5	$C_2 + H_2 \rightleftharpoons C_2H + H$	6.60×10^{13}	0.	8 000.	s.t.
6	$C_2H + H_2 \rightleftharpoons C_2H_2 + H$	7.40×10^{14}	0.	6 700.	s.t.
7	$C_4 \rightarrow 4C(s)$	8.00×10^{3}	0.	0.	s.t.
8	$C + CH \rightleftharpoons C_2 + H$	5.00×10^{14}	0.	0.	est.
9	$C + C_2H \rightleftharpoons C_3 + H$	7.00×10^{14}	0.	0.	est.
10	$C + C_2H_2 \rightleftharpoons C_3H + H$	4.00×10^{14}	0.	12 000.	29
11	$C_2 + CH \rightleftharpoons C_3 + H$	2.00×10^{14}	0.	0.	29
12	$C_2 + C_2H \rightleftharpoons C_4 + H$	1.20×10^{14}	0.	0.	28
13	$C_2 + C_2H_2 \rightleftharpoons C_4H + H$	1.00×10^{14}	0.	0.	28
14	$C_2 + C_4H \rightleftharpoons C_2H + C_4$	1.20×10^{14}	0.	0.	28
15	$C_2 + C_4H \rightleftharpoons C_6 + H$	1.20×10^{14}	0.	0.	28
16	$C_2 + C_4H_2 \rightleftharpoons C_6H + H$	1.20×10^{14}	0.	0.	28
17	$C_2 + C_6H \rightleftharpoons C_2H + C_6$	1.20×10^{14}	0.	0.	28
18	$C_4 + C_2H \rightleftharpoons C_6 + H$	1.20×10^{14}	0.	0.	28
19	$C_4 + C_6H \rightleftharpoons C_4H + C_6$	1.20×10^{14}	0.	0.	28
20	$CH + H \rightleftharpoons C + H_2$	1.10×10^{14}	0.	0.	29
21	$CH + CH \rightleftharpoons C_2 + H + H$	1.00×10^{14}	0.	0.	29
22	$CH_2 + H \rightleftharpoons CH + H_2$	1.10×10^{14}	0.	0.	29
23	$C_2H + C_2H \rightleftharpoons C_2H_2 + C_2$	1.00×10^{13}	0.	0.	28
24	$C_2H + C_2H \rightleftharpoons C_4H + H$	1.00×10^{14}	0.	0.	28
25	$C_2H + C_2H_2 \rightleftharpoons C_4H_2 + H$	5.00×10^{14}	0.	0.	est.
26	$C_2H + C_4H_2 \rightleftharpoons C_4H + C_2H_2$	1.00×10^{13}	0.	0.	28
27	$C_2H + C_4H_2 \rightleftharpoons C_6H_2 + H$	1.20×10^{14}	0.	0.	28
28	$C_2H + C_6H \rightleftharpoons C_6 + C_2H_2$	1.00×10^{13}	0.	0.	28
29	$C_2H + C_6H \rightleftharpoons C_2 + C_6H_2$	1.20×10^{14}	0.	0.	28
30	$C_2H_2 + C_2H_2 \rightleftharpoons C_4H_2 + H_2$	1.50×10^{13}	0.	42 700.	28
31	$C_2H_2 + C_2H_2 \rightleftharpoons C_4H_3 + H$	1.50×10^{14}	0.	56 000.	28
32	$C_2H_2 + C_4H \rightleftharpoons C_6H_2 + H$	1.20×10^{14}	0.	0.	28
33	$C_2H_2 + C_6H \rightleftharpoons C_8H_2 + H$	1.20×10^{14}	0.	0.	28
34	$C_3H + H \rightleftharpoons C_3 + H_2$	1.00×10^{14}	0.	0.	29
35	$C_3H_2 + H \rightleftharpoons C_3H + H_2$	6.31×10^{13}	0.	0.	29
36	$C_4H + H \rightleftharpoons C_4 + H_2$	2.00×10^{13}	0.	0.	28
37	$C_4H + H_2 \rightleftharpoons C_4H_2 + H$	4.07×10^{5}	2.4	200.	28
38	$C_4H + C_4H \rightleftharpoons C_4 + C_4H_2$	1.20×10^{14}	0.	0.	28
39	$C_4H + C_4H_2 \rightleftharpoons C_8H_2 + H$	1.20×10^{14}	0.	0.	28
40	$C_4H + C_6H \rightleftharpoons C_4 + C_6H_2$	1.20×10^{14}	0.	0.	28
41	$C_4H + C_6H \rightleftharpoons C_4H_2 + C_6$	1.00×10^{13}	0.	0.	28
42	$C_4H + C_6H_2 \rightleftharpoons C_4H_2 + C_6H$	1.00×10^{13}	0.	0.	28
43	$C_4H + C_8H \rightleftharpoons C_4 + C_8H_2$	1.00×10^{13}	0.	0.	28
44	$C_6H + H \rightleftharpoons C_4 + C_2H_2$	1.00×10^{14}	0.	0.	28
45	$C_6H + H \rightleftharpoons C_6 + H_2$	2.00×10^{13}	0.	0.	28
46	$C_6H + H_2 \rightleftharpoons C_6H_2 + H$	4.07×10^{5}	2.4	200.	28
47	$C_6H + C_6H \rightleftharpoons C_6H_2 + C_6$	1.00×10^{13}	0.	0.	28
48	$C_6H_2 \rightleftharpoons C_6H + H$	6.00×10^{13}	0.	0.	28
49	$H + C_4 + M \rightleftharpoons C_4H + M$	1.74×10^{37}	−5.5	0.	28
50	$C_4H_2 \rightleftharpoons C_4H + H$	1.30×10^{8}	2.2	122 600.	28
51	$C_3 + M \rightleftharpoons C_2 + C + M$	4.00×10^{16}	0.	150 000.	29
52	$C_2 + C_2 + M \rightleftharpoons C_4 + M$	1.00×10^{27}	−3.0	0.	28
53	$CH + M \rightleftharpoons C + H + M$	1.90×10^{14}	0.	66 968.	35
54	$CH_2 + M \rightleftharpoons C + H_2 + M$	1.15×10^{14}	0.	55 820.	29
55	$CH_2 + M \rightleftharpoons CH + H + M$	2.88×10^{14}	0.	79 030.	29
56	$CH_3 + M \rightleftharpoons CH_2 + H + M$	1.58×10^{15}	0.	76 610.	29
57	$C_3H + M \rightleftharpoons C_3 + H + M$	1.58×10^{14}	0.	39 420.	29
58	$C_3H_2 + M \rightleftharpoons C_3H + H + M$	1.00×10^{15}	0.	60 000.	29
59	$C_2 + C_4H + M \rightleftharpoons C_6H + M$	2.09×10^{23}	−3.0	0.	28
60	$H_2 + M \rightleftharpoons H + H$	2.23×10^{14}	0.	96 080.	34

[a] Rate coefficient $k = AT^n \exp(-E_A/RT)$.

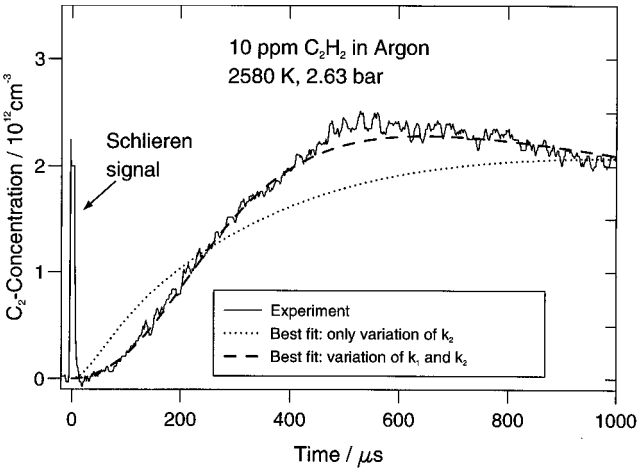

Figure 8. Measured and calculated C_2 concentration profile obtained at relatively low temperature. The dotted line shows the best simulation using the literature value for k_1 varying only k_2. The dashed lines shows the best simulation fitting obtained by varying both k_1 and k_2.

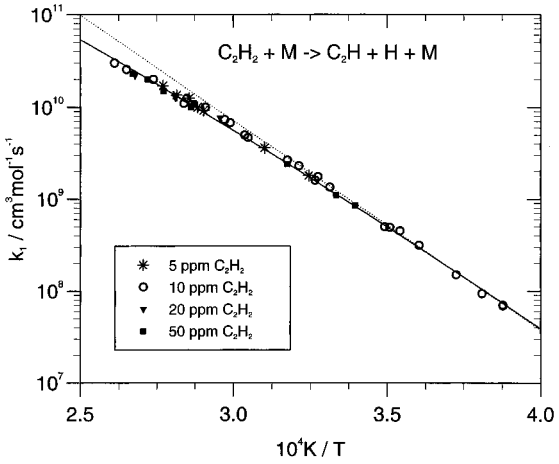

Figure 9. Rate coefficient of the reaction $C_2H_2 + M \rightleftharpoons C_2H + H + M$. The dotted line corresponds to the Arrhenius expression and the solid line to a modified Arrhenius expression (see text).

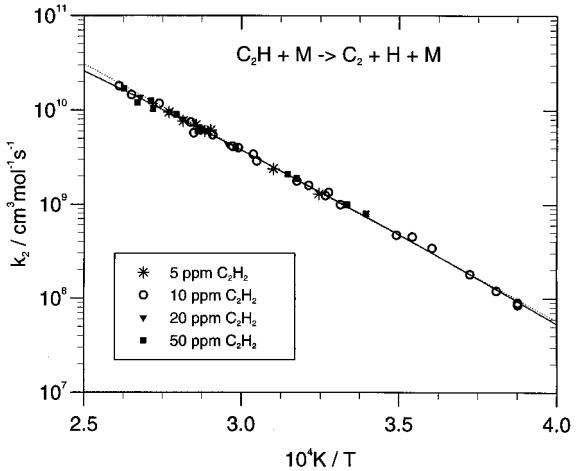

Figure 10. Rate coefficient of the reaction $C_2H + M \rightleftharpoons C_2 + H + M$. Dotted line, Arrhenius expression; solid line, modified Arrhenius expression.

important species used for our kinetic modeling are shown in Table 3. Again a satisfactory fit of the measured C_2 profiles could only be obtained with the earlier suggested change in the thermodynamics of C_2. An additional modification of the thermodynamic properties of C_4 was also suitable. The best fit was achieved by reducing the Gibbs free energy of C_4 by about 20 kcal mol^{-1} compared to the value given by Burcat.[30]

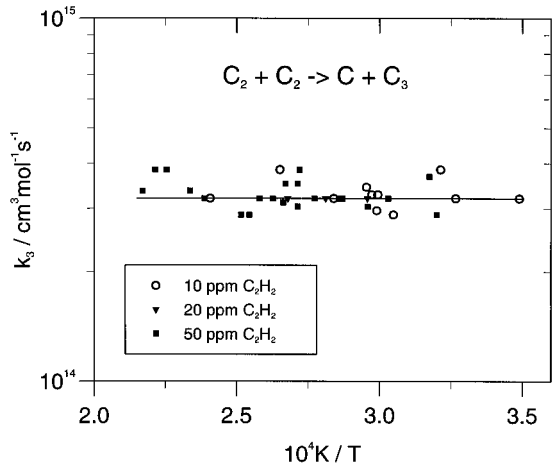

Figure 11. Rate coefficient of the reaction $C_2 + C_2 \rightleftharpoons C + C_3$.

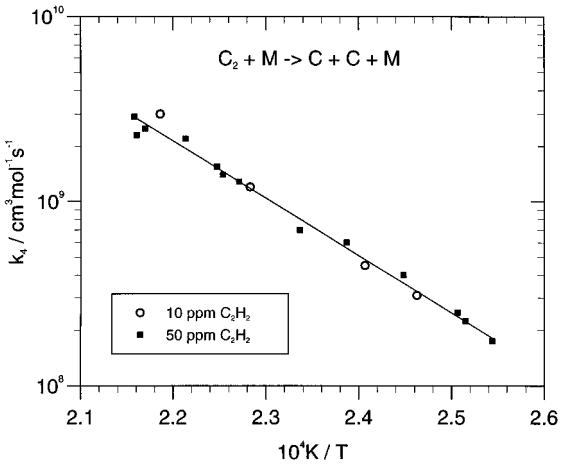

Figure 12. Rate coefficient of the reaction $C_2 + Ar \rightleftharpoons C + C + M$.

TABLE 3: Thermodynamic Data at Room Temperature and 3500 K of Some Important Species Used for the Kinetic Modeling

species	$S°_{298.15}$ (cal/mol/K)	$S°_{3500}$ (cal/mol/K)	$H°_{298.15}$ (kcal/mol)	$H°_{3500}$ (kcal/mol)	ref
H	27.4	39.6	52.1	68.0	20
C	37.8	50.1	171.3	187.5	20, 1
C_2	47.6	70.1	194.7	224.4	s.t.
C_2H	49.6	79.7	135.0	178.4	20
C_2H_2	48.0	88.2	54.2	113.0	20
C_3	56.7	83.2	196.0	233.5	20, 1
C_3H	54.2	91.8	163.5	219.6	30
C_4	60.4	111.8	247.1	311.7	s.t.
C_4H	63.5	117.8	192.0	268.6	30
C_6	57.9	113.2	282.2	360.7	30
C_6H	74.1	154.1	213.2	326.6	20

This can be achieved, e.g., by increasing the entropy of C_4 by 5.7 cal mol^{-1} K^{-1} or 6% compared to the value given by Burcat.[30] The possibility of a too low literature value of the C_4 entropy was already discussed by Kiefer et al.[28] on the basis of experiments performed by Heath et al.[31] An example illustrating the different effects is shown in Figure 13. The experimental conditions are $T = 3492$ K, $p = 2.14$ bar, and 500 ppm C_2H_2 diluted in Ar. The noisy line comes from the experiment, the dotted line represents a calculation with the Burcat value for the entropy of C_4, and the dashed line was calculated with the modified C_4 data. A nearly perfect agreement, see the dashed dotted line, with the experimental profile even at later reaction time was achieved by assuming the formation of solid carbon. Following the suggestion of Kiefer et al.,[32] reaction R7 was introduced which converts in an irreversible way C_4 into solid carbon. Similar good agreement

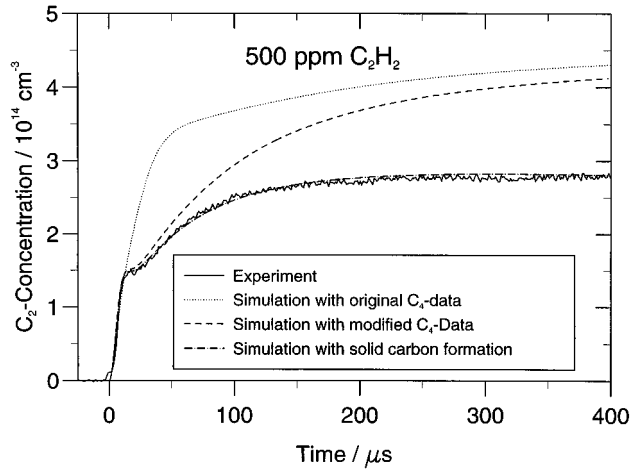

Figure 13. Comparison of different models used to describe the measured C_2 concentration for an experiment 500 ppm C_2H_2 diluted in Ar, $T = 3490$ K and $p = 21.4$ bar.

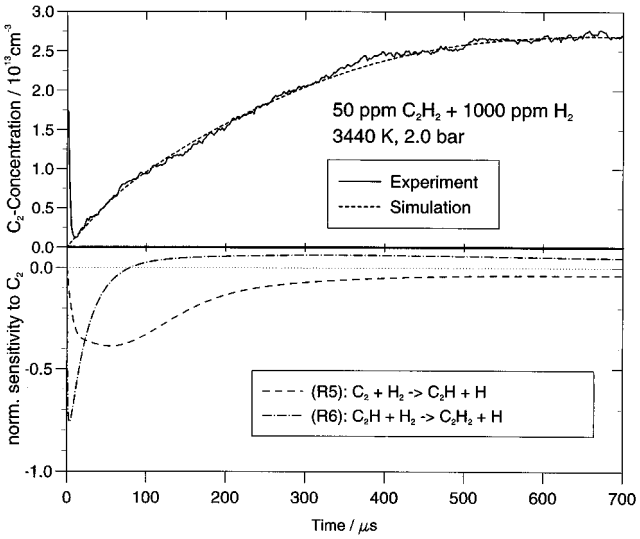

Figure 14. (upper) Measured and calculated C_2 profiles during the pyrolysis of 50 ppm C_2H_2 diluted in Ar enriched with 1000 ppm H_2. (lower) Normalized sensitivity coefficients of the H_2 perturbation reactions R5 and R6 describing the influence on the C_2 concentration for this experiment.

was also obtained for the other experiments; see Figure 6, dashed lines. The best fit rate coefficient used during the computer simulation was $k_7 = (8 \pm 3) \times 10^3$ s^{-1}.

The last group of results includes five experiments of 20 ppm C_2H_2 diluted in Ar and five experiments of 50 ppm C_2H_2 diluted in Ar enriched with 1000 ppm H_2. We again started our computer simulation on the basis of the complete mechanism consisting of 145 reactions. It is obvious that now reactions R5 and R6

$$C_2 + H_2 \overset{k_5}{\rightleftharpoons} C_2H + H \qquad \text{(R5)}$$

$$C_2H + H_2 \overset{k_6}{\rightleftharpoons} C_2H_2 + H \qquad \text{(R6)}$$

have a high sensitivity to the C_2 concentration. As can be seen in Figure 14, both reactions are responsible for the drastic slowdown of the C_2 rise, whereby reaction R6 is most sensitive in the first 50 μs and reaction R5 in the following 200 μs. Thus, both rate coefficients can be evaluated seperately on the basis of computer fittings of the experimental C_2 concentrations by varying the rate coefficients k_5 and k_6. Individual results obtained from fittings at early reaction time are summarized in

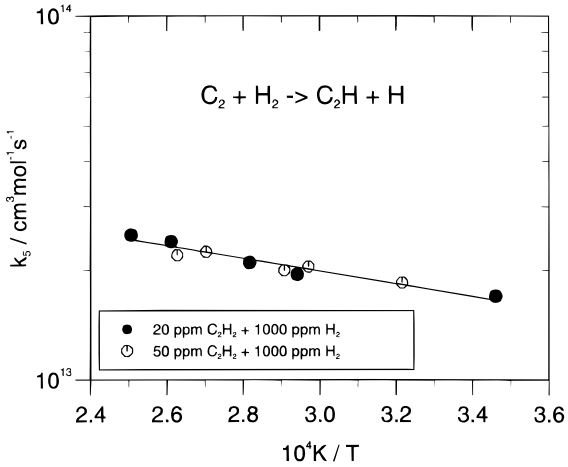

Figure 15. Rate coefficient of the reaction $C_2 + H_2 \rightleftharpoons C_2H + H$.

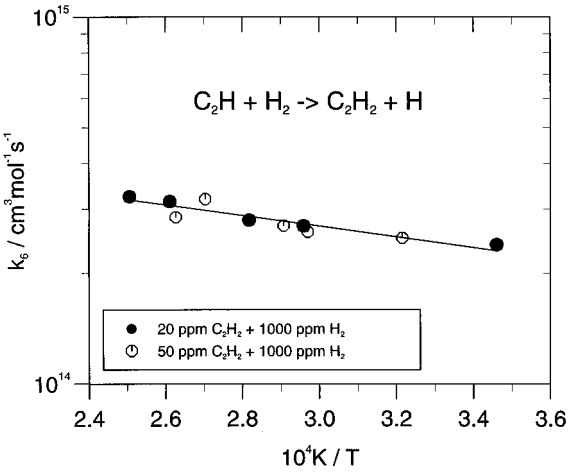

Figure 16. Rate coefficient of the reaction $C_2H + H_2 \rightleftharpoons C_2H_2 + H$.

the Figures 15 and 16. The points can be approximated by the Arrhenius expressions:

$$k_5 = 6.6 \times 10^{13} \exp(-4000/T) \text{ cm}^3 \text{ mol}^{-1} \text{ s}^{-1}$$

$$k_6 = 7.4 \times 10^{14} \exp(-3400/T) \text{ cm}^3 \text{ mol}^{-1} \text{ s}^{-1}$$

The rate coefficient k_5 has not been measured before in the high-temperature regime, but the value is in accordance with an estimation by Kiefer et al.[28] Our value for k_6 is at 3000 K by factor of 20 higher than the value recomended by Baulch et al.[33] An estimated value by Kiefer et al.[28] and a value obtained from the backward reaction of R6 measured by Frank and Just[6] are relatively close to our value.

The nearly perfect agreement of the simulations with the experimental profiles (see Figure 5) for the whole measurement time of 1000 μs could only be obtained by including the complete mechanism of Table 2. The slow disappearance of the C_2 at later reaction times in the higher temperature experiments is mainly due to reactions involving H, C, C_2, and CH as, for example reactions, R8, R9, and R53. The rate coefficients of this three reactions and the rate coefficients of reactions R12 and R25 were adjusted in a range of ±30% compared to the values given in Table 2 to obtain best agreement between experiment and simulation. For the H_2 dissociation, which is also very sensitive to the C_2 profiles at later reaction time, the rate coefficient recommended by Baulch et al.[34] was used. Again, the thermodynamic properties of the species listed in Table 3 proved to be very important, and we found that the best fit was again possible with the above suggested changes in the thermodynamics of C_2 and C_4.

Conclusion

C_2 measurements during high-temperature pyrolysis of acetylene diluted in Ar covering the temperature range of 2580−4650 K could be verified in a wide range of mixture compositions by a consistent mechanism of 60 reactions. In the very low concentration range of 50 ppm C_2H_2 or less, a simplified description of the measured C_2 profiles could be given on the basis of four elementary reactions, for which rate coefficients were evaluated. A discrepancy in the JANAF thermodynamic data[1] of either C, C_2, or C_3 was revealed and tentatively explained by a reduction of the JANAF $\Delta_f H^0_{298.15}$ value for C_2 by about 5.5 kcal/mol. In a series of experiments with higher C_2H_2 concentrations up to 500 ppm, a complex mechanism of 145 reactions was checked and reduced by sensitivity analysis to 60 elementary reactions. The simulation of the experiments showed a high sensitivity to the thermodynamic properties of the involved species, especially C_2, and C_4. With slight modification in the thermodynamic properties of this species and an assumed conversion of C_4 into solid carbon, the measured C_2 concentration profiles could nearly perfectly be fitted. In a perturbation study with addition of H_2, rate coefficients for the reactions $C_2 + H_2 \rightleftharpoons C_2H + H$ and $C_2H + H_2 \rightleftharpoons C_2H_2 + H$ could be determined. In general we found that an accurate knowledge of the thermodynamic data of the involved species is crucial for a correct description of the acetylene pyrolysis.

Acknowledgment. The authors thank Mrs. C. Kmiecik, Mrs. N. Schlösser, and Mr. L. Jerig for their help in conducting the experiments. We also thank Prof. Th. Just, DLR Stuttgart, for helpful discussion. The financial support of the Deutsche Forschungsgemeinschaft is gratefully acknowledged.

References and Notes

(1) Chase, M. W., Jr.; Davies, C. A.; Downey, J. R.; Frurip, D. J.; McDonald, R. A.; Syverud, A. N. JANAF thermochemical tables. *J. Phys. Chem. Ref* **1985**, 14.

(2) Gaydon, A. G.; Wolfhard, H. G. *Flames*; Chapman and Hall, New York, 1979.

(3) Perry, M. D.; Raff, L. M. *J. Phys. Chem.* **1994**, *98*, 4375−4381.

(4) O'Brien, S. C.; Heath, J. R.; Curl, R. F.; Smalley, R. E. *J. Chem. Phys.* **1988**, *88*, 220−230.

(5) Beck, W. H.; Mackie, J. C. *J. Chem. Soc., Faraday Trans.* **1975**, *71*, 1363−1371.

(6) Frank, P.; Just, T. *Combust. Flame* **1980**, *38*, 231−248.

(7) Kern, R. D.; Xie, K.; Chen, H.; Kiefer, K. J. H. High Temperature Pyrolysis of Acetylene and Diacetylene Behind Reflected Shock Waves. *23th Symposium (International) on Combustion*; The Combustion Institute: Pittsburgh, 1990; pp 69−75.

(8) Phillips, J. G.; Davis, S. P. *The Swan System of The C_2 Molecule, Berkeley Analysis of Molecular Spectra*; University of California Press: Berkeley, Los Angeles, 1984.

(9) Sviridov, A. G.; Sobolev, N. N.; Novgorodev, M. Z.; Arytyunova, G. A. *J. Quant. Spectrosc. Radiat. Transfer* **1966**, *6*, 875−892.

(10) Naulin, C.; Costes, M.; Dorthe, G. *Chem. Phys. Lett.* **1988**, *143*, 496−500.

(11) Bauer, W.; Bielefeld, M.; Becker, K. H.; Meuser, R. *Chem. Phys. Lett.* **1986**, *123*, (1,2), 33−36.

(12) Stark, G.; Davis, S. P. *Z. Phys. A: At. Nucl.* **1985**, *321*, 75−77.

(13) Arnold, J. O. *J. Quant. Spectrosc. Radiat. Transfer* **1968**, *8*, 1781−1794.

(14) Cooper, D. M.; Nicholls, R. W. *J. Quant. Spectrosc. Radiat. Transfer* **1975**, *15*, 139−150.

(15) Kruse, T.; Roth, P. To be published.

(16) Von Gersum, S.; Kruse, T.; Roth, P. *Ber. Bunsen-Ges. Phys. Chem.* **1994**, *98*, 979−982.

(17) Kiess, N. H.; Broida, H. P. *Can. J. Phys.* **1956**, *34*, 1471−1479.

(18) Becker, K. H.; Tatarczyck, T. *Chem. Phys. Lett.* **1979**, *60*, 502−506.

(19) Danylewych, L. L.; Nicholls, R. W. *Proc. R. Soc. London A* **1974**, *339*, 197−222.

(20) Kee, R. J.; Rupley, F. M.; Miller, J. A. The CHEMKIN Thermodynamic Data Base. SANDIA REPORT, SAND95-8215; Sandia National Laboratories: Albuquerque, NM, 1995.

(21) Urdahl, R. S.; Jackson, W. M.; Bao, Y.; *Chem. Phys. Lett.* **1991**, *178*, 425−428.

(22) Bauschlicher, C. W., Jr.; Langhoff, S. R. *Chem. Phys. Lett.* **1990**, *173*, 367−370.

(23) Warnatz, J. Rate Coefficients in the C/H/O-System. In *Combustion Chemistry*; Gardiner, W. C., Jr., Ed.; Springer-Verlag: New York, 1984.

(24) Ervin, K. M.; Gronert, S.; Barlow, S. E.; Gilles, M. K.; Harrision, A. G.; Bierbaum, V. M.; Ellison, G. B. *J. Am. Chem. Soc.* **1990**, *112*, 5750.

(25) Bauschlicher, C. W., Jr.; Langhoff, S. R. *Astrophy. J.* **1988**, *332*, 531.

(26) Kordis, J.; Gingerich, K. A. *J. Chem. Phys.* **1973**, *58*, 5058.

(27) Gaydon, A. G.; Wolfhard, H. G. *Dissociation Energies and Spectra of Diatomic Molecules*; Chapman and Hall: London, 1968.

(28) Kiefer, J. H.; Sidhu, S. S.; Kern, R. D.; Xie, K.; Chen, H.; Harding, L. B. *Combust. Sci. Technol.* **1992**, *82*, 101−130.

(29) Kiefer, J. H.; Kumaran, S. S. *J. Phys. Chem.* **1993**, *97*, 414−420.

(30) Burcat, A.; McBride, B. *1994 Ideal Gas Thermodynamic Data for Combustion and Air-Pollution Use*; TECHNION-Israel Institute of Technology, Faculty of Aerospace Engineering, Haifa, 1994.

(31) Heath, J. R.; Saykally, R. J. *J. Chem. Phys.*, **1991**, *94*, 3271.

(32) Kiefer, J. H.; Kapsalis, S. A.; Al-Alami, M. Z.; Budach, K. A. *Combust. Flame* **1983**, *51*, 79−93.

(33) Baulch, D. L.; Cobos, C. J.; Cox, R. A.; Frank, P.; Hayman, G.; Just, Th.; Kerr, J. A.; Murrells, T.; Pilling, M. J.; Troe, J.; Walker, R. W.; Warnatz, J. *Combust. Flame* **1994**, *98* (Suppl. 1), 59−79.

(34) Baulch, D. L.; Cobos, C. J.; Cox, R. A.; Esser, C.; Frank, P.; Just, Th.; Kerr, J. A.; Pilling, M. J.; Troe, J.; Walker, R. W.; Warn, J. *J. Phys. Chem. Ref. Data* **1992**, *21*, 411−429.

(35) Dean, A. J.; Hanson, R. K. *Int. J. Chem. Kinet.* **1992**, *24*, 517−532.